The Antiproton Source Target Station was originally designed to produce 8 GeV antiprotons from an incident target beam of 120 GeV protons with a peak beam power of about 20 kW. Over its 25 year operating history, numerous design improvements, both at the target station and across the accelerator complex, led to the eventual target station operation with a beam power of 70 kW. Perhaps even more importantly, the duty factor for the target station operation during running periods increased from about 60% to greater than 95%. The Target Station performed well beyond those early design expectations during the Tevatron Collider program; indeed, collectively, the Antiproton Source set pbar production records that may never be realized again.

While the Tevatron Collider program has been ended, the target station is anticipated to be repurposed for the Muon g-2 experiment. In the conceptual design, the proton beam energy on target is reduced from 120 GeV to 8 GeV. The average number of protons incident on target for pbar production was about 3.64E12 p/s while for muon g-2 the number will be about 1.2E13 p/s. The secondary beam produced changes from 8.9 GeV/c antiprotons to 3.1 GeV/c positive pions. The incident beam power on target is reduced from 70 kW to about 15 kW. Regardless of its outstanding performance during the Tevatron Collider program, many new questions must now be answered about how the Target Station may perform for the Muon g-2 experiment. There are two central questions:

1. Can the target station produce sufficient pion yield to satisfy the needs of the Muon g-2 experiment?
2. Are the individual target station component designs adequate for the Muon g-2 experiment.

The focus of the remainder of this paper is on the second question. The first question is being addressed separately in a parallel effort. The major components addressed in this paper are the production target, collection lens/transformer assembly, the collimator, the pulsed magnet, and the beam dump. Figure 1 presents a graphical representation of the MARS model for the pbar target station used in the discussions within this paper.

Production Target

A series of MARS calculations has been made to study the energy deposition in Inconel 600 targets for pbar production and for positive and negative pion production for the Muon g-2 experiment. Salient model parameters and results are included in Table 1. The modeled target volume is a simple 1 bin, solid cylinder, an approximation of the actual design. Energy deposition is averaged over the entire volume, i.e., one bin and normalized to beam power on target. The resulting beam heating calculation should yield a valid, macroscopic comparison of the two operating modes.

Energy GeV/pion sign	Beam σ_x, σ_y (mm)	Protons/s	Component volume (cc)	Component density (g/cc)	Component mass (g)	Energy Density (GeV/g-p)	% error	kW
120	0.2	3.64E12	3078	8.19	25,210	7.917E-5	0.46	1.2
8/+	0.2	1.2E13	3078	8.19	25,210	1.929E-5	0.3	0.9
8/-	0.2	1.2E13	3078	8.19	25,210	1.925E-5	0.3	0.9

TABLE 1: Target heating for pbar and pion production operating modes

There are two results to consider. First, on average, the beam power absorbed by the target is 25% lower for pion production than for pbar production. Second, assuming a 0.2 mm σ beam spot size, the beam passes through a chord volume of about 0.063 cc instantaneously in the pbar production case. For the pion production case, the target rotates about 8 degrees in one second while twelve 1E12 proton batches are delivered. Microscopically, the energy density in the 0.063 cc volume should be a factor of 2 to 4 lower for the pion production case. (Some overlapping of the chords will occur because the 1E12per pulse beam is delivered in four 100 Hz, four pulse bursts every 1.33 seconds). Both of these factors suggest the existing pbar production target would perform suitably as a mechanical structure for the Muon g-2 experiment.

In this analysis, there are four important design features associated with the pbar production target which are assumed to be maintained for target station operation for Muon g-2 in order to sustain target lifetime.

1. The target is air cooled by an air blower with a 30 SCFM flow rate.
2. The target is continuously rotated with a period of 45 seconds to prevent prolonged energy deposition in any particular location.
3. A beryllium cover excludes air from the surface of the target to prevent oxidation of the target surface.
4. The target cylinder vertical position is automatically changed by a Controls System ACL script about 1 mm (roughly 6 σ) after every 2E17 protons.

Lithium Lens and transformer

From a simple scaling exercise, it has been determined that the lithium lens should be able to pulse at an average of 12 Hz if the lens gradient is reduced by the ratio of the respective secondary particle momenta. There are two efforts going on to determine if the lithium lens and transformer can work for the Muon g-2 experiment. First, 12 Hz lens pulse testing was begun in July 2012. Power supply heating issues have been found and fixed as peak current in the collection lens has been gradually increased to 18 kA. A new 40 kW, 480/380 VAC transformer is required to source the collection lens test station power supply (PPS100). The goal of lens pulse testing is to achieve 19.25 kA peak current in the collection lens primary circuit (154 kA peak current in the lens) which should be equivalent to a gradient of about 230 T/m in the lithium conductor. Second, an ANSYS analysis of collection lens heating has been performed to model the anticipated heating. Preliminary results to date are that the ANSYS model and test results agree remarkably well.

A MARS calculation for the energy deposition due to beam heating in the lithium lens is required to complete the ANSYS thermal model. An energy deposition calculation for a simple, 1 bin model of the lithium lens substructure has been made in a MARS calculation for the pbar production case and for the +/- pion production case. Salient model parameters and results are included in Table 2. A MARS histogram of energy deposition in the entire collection lens, normalized to beam power for the three scenarios given in Table 2, is shown in Figure 2, a 50 X 50 bin array. It is clear that total energy deposition is down by a factor of about 4 in the pion production cases compared with the pbar production case.

lens material	120 GeV pbar production (kW)	8 GeV positive pion production (kW)	8 GeV negative pion production (kW)
usendcap	1.24E-01	2.78E-02	2.76E-02
usBe	4.36E-02	1.55E-02	1.54E-02
usFE-BE	5.79E-02	1.92E-02	1.83E-02
usTiWin	5.49E-04	1.83E-04	1.80E-04
mainLi	4.43E-02	2.36E-02	2.47E-02
usLishor	1.41E-03	3.06E-04	2.80E-04
usLilong	3.26E-03	7.59E-04	7.37E-04
Tiinner	3.73E-02	8.71E-03	8.35E-03
waterinn	2.12E-02	4.79E-03	4.83E-03
currdiv	8.64E-02	1.47E-02	1.46E-02
waterout	9.96E-03	1.96E-03	1.98E-03
Tiouter	7.43E-02	1.21E-02	1.19E-02
ussteeld	2.68E-02	5.32E-03	5.09E-03
usmiscst	3.83E-02	8.26E-03	8.08E-03
usouterF	2.41E-01	7.24E-02	7.07E-02
Tioutbod	7.81E-02	1.32E-02	1.31E-02
ceramic	1.51E-02	2.98E-03	2.84E-03
dssteeld	3.83E-02	5.97E-03	5.85E-03
dsLilong	5.01E-03	8.86E-04	9.04E-04
dsLishor	2.02E-03	4.16E-04	4.03E-04
dsmiscst	4.86E-02	8.77E-03	8.74E-03
dsouterF	2.60E-01	6.60E-02	6.56E-02
dsTiWin	0.00E+00	0.00E+00	0.00E+00
cyl-4	3.38E-02	1.32E-02	1.34E-02
dsFE-BE	8.40E-02	1.91E-02	1.91E-02
dsendcap	1.63E-01	3.20E-02	3.26E-02
Totals	1.54	0.38	0.38

Table 2

Beam heating in the collection lens transformer is considered in Table 3. A MARS Histogram of energy deposition in the transformer, normalized to beam power on target for the three scenarios given in Table 3, is shown in Figure 3, a 50 X 50 bin array. Overall, beam heating in the transformer is lower by about 25% for the pion production cases compared with the pbar production cases. However, there are portions of the transformer assembly that receive a disproportionate fraction of the energy deposited by the beam in the pion production case. Internally cooled transformers are capable of rapidly removing heat except for the case of the transformer core which is both rather massive and is also insulated from the internally cooled, aluminum secondary housing. The MARS calculations shows that the transformer core beam heating is similar for the pbar production and muon g-2 pion production cases.

Electrical (joule) heating of the lens and transformer will increase significantly for pion production over that which occurred for pbar production. Test station data is required to predict the total lens and transformer heating to be expected for pion production. Total heating in the lens and transformer are considered further, below.

xfmr material	120 GeV pbar production (kW)	8 GeV positive pion production (kW)	8 GeV negative pion production (kW)
usfinger	8.12E-03	3.44E-03	3.36E-03
usfingex	4.05E-03	2.14E-03	2.12E-03
usinhous	1.23E-01	7.98E-02	7.94E-02
usfeclam	4.63E-02	2.64E-02	2.63E-02
usfacedi	1.30E-02	1.10E-02	1.09E-02
usdsouth	2.16E-02	2.77E-02	2.79E-02
outerear	3.36E-03	4.42E-03	4.34E-03
ironcore	**1.85E-01**	**1.79E-01**	**1.78E-01**
dsear	2.09E-03	2.02E-03	2.05E-03
dsfacedi	9.61E-03	7.14E-03	7.30E-03
dsinhous	1.16E-01	7.50E-02	7.49E-02
dsfingex	3.73E-03	1.95E-03	1.90E-03
dsfinger	8.53E-03	3.54E-03	3.53E-03
dsfeclam	6.10E-02	3.02E-02	2.99E-02
Totals	0.61	0.45	0.45

Table 3: Transformer component beam heating for three beam scenarios. Beam heating in the transformer core for pion production cases is similar to the 120 GeV pbar production case. The transformer core is electrically/thermally insulated from the water cooled secondary housing.

Collimator

The purpose of the collimator is to limit energy deposition in the pulsed magnet. Several efforts were made in the mid-2000s to extend the lifetime of the pulsed magnet including:

1. Improved conductor bar connections (timeserts)
2. Removal of torlon interference between crossover plate and conductor bars
3. Design and installation of collimator
4. Replacement of selected torlon insulators with ceramic ones
5. Horizontal alignment change (to right of beam path) to move remnant primary beam from the beam right primary conductor bar

The value of the individual efforts could not be quantified because they occurred more or less simultaneously. Altogether, the result was that pulsed magnet lifetime was extended from 2 to 4 months to about 2 years with a factor of 4 to 5 increase in pulse life and a factor of 5 to 10 increase in protons on target over the service life. The collimator certainly played a major role in extending the lifetime of the pulsed magnet. Typical beam heat removal by the collimator was about 7 kW; without the collimator in place this heat would have been absorbed, mostly by the pulsed magnet and somewhat by the beam dump.

Results of MARS collimator calculations for the pbar and pion production cases are shown in Figure 4, a histogram of a 50 X 50 bin array, 1 bin deep representing the entire mass of the collimator.

The beam power deposited in the collimator is also calculated from MARS energy deposition results for the pbar production case and the pion production cases. Tables 4 and 5 show the salient parameters for this calculation. The calculated total heat deposited in the collimator is the sum of the power from the two tables.

Energy GeV/pion sign	Beam σ_x, σ_y (mm)	Protons/s	Component volume (cc)	Component density (g/cc)	Component mass (g)	Energy Density (GeV/g-p)	% error	kW
120	0.2	3.64E12	2003	8.96	17,949	3.554E-04	0.43	3.72
8/+	0.2	1.2E13	2003	8.96	17,949	1.535E-05	0.65	0.53
8/-	0.2	1.2E13	2003	8.96	17,949	6.058E-06	1.1	0.60

Table 4: Upstream half of collimator beam heating

Energy GeV/pion sign	Beam σ_x, σ_y (mm)	Protons/s	Component volume (cc)	Component density (g/cc)	Component mass (g)	Energy Density (GeV/g-p)	% error	kW
120	0.2	3.64E12	1975	8.96	17,700	1.551E-04	0.66	1.60
8/+	0.2	1.2E13	1975	8.96	17,700	6.058E-06	1.1	0.21
8/-	0.2	1.2E13	1975	8.96	17,700	9.074E-06	0.86	0.31

Table 5: Downstream half of collimator beam heating

Total beam heating in the collimator for the three cases is collected in Table 6.

Energy (GeV)/pion sign	kW
120	5.32
8/+	0.74
8/-	0.91

Table 6: Total beam heating in collimator

Beam heating in the collimator for muon g-2 pion production will be significantly lower than that for the pbar production mode.

Pulsed Magnet

A MARS model of the pulsed magnet and histograms of energy deposition normalized to beam on target for the three operating modes is shown in Figure 5. The results of the energy deposition calculation for the three operating modes as a function of material in the pulsed magnet is shown in Table 7.

Pmag material	120 GeV pbar production (kW)	8 GeV positive pion production (kW)	8 GeV negative pion production (kW)
Left copper conductor	0.747	0.030	0.292
Right copper conductor	0.178	0.012	0.034
Left side torlon	0.010	0.001	0.006
Left upper torlon	0.013	0.001	0.008
Left lower torlon	0.013	0.001	0.007
Right side torlon	0.003	0.000	0.001
Right upper torlon	0.004	0.000	0.001
Right lower torlon	0.004	0.000	0.001
Ti nuts left	0.051	0.004	0.023
Ti nuts right	0.010	0.001	0.002
Left side lamination	0.274	0.027	0.159
Right side lamination	0.133	0.020	0.049
Top lamination	1.663	0.222	0.686
Bottom lamination	1.672	0.225	0.683
Totals	**4.777**	**0.545**	**1.953**

Table 7: Pulsed magnet beam heating under pbar production conditions and under pion production conditions.

Pulsed magnet joule heating was monitored during testing of new units on the test stand. Joule heating was found to be quite insignificant, certainly less than 200 watts. Joule heating will be measured for the pion production case when the pulsed magnet is eventually tested on the test stand under muon g-2 operating conditions. Joule heating of the pulsed magnet is not expected to be an issue. Beam heating is substantially reduced in the muon g-2 operating mode.

Beam Dump

The MARS model of a small portion of the existing beam dump along with the MARS histogram is shown in Figure 6. The dump core consists of a graphite cylinder, 6” in diameter and 48” long. Behind the graphite core is an aluminum backstop about 40” long. In the model, an aluminum cylinder, 10.5” in diameter surrounds the graphite and the aluminum backstop. While the aluminum cylinder and backstop are modeled as separate parts, they are in fact one piece, i.e., an aluminum cylinder, 10.5” in diameter by 87” long with a 6” diameter boring, 48” long which accommodates the graphite core. In the model, the aluminum cylinder is contained within a 31” diameter iron cylinder, also 87” long. In reality, the steel extends outward radially and longitudinally. This model approximates the reach of the existing beam dump water cooling system. Salient parameters of the beam along with energy deposition results for the three cases are shown in Tables 8, 9, and 10. MARS histograms for the three cases are also shown in Figure 6.

Protons/s	component	Component volume (cc)	Component density (g/cc)	Component mass (g)	Energy Density (GeV/g-p)	kW	% error
3.64E+12	graphite	21,890	1.7	3.721E+04	1.73E-04	3.75	0.39
3.64E+12	Al back	18,241	2.7	4.925E+04	3.47E-04	9.95	0.39
3.64E+12	Al cylinder	82,863	2.7	2.237E+05	4.49E-05	5.85	0.33
3.64E+12	Fe cylinder	982,847	7.86	7.725E+06	2.25E-06	10.14	0.32
					Total	29.7	

Table 8: beam dump energy deposition for pbar production case

Protons/s	component	Component volume (cc)	Component density (g/cc)	Component mass (g)	Energy Density (GeV/g-p)	kW	% error
1.20E+13	graphite	21,890	1.7	3.72E+04	1.06E-05	0.76	0.34
1.20E+13	Al back	18,241	2.7	4.93E+04	2.88E-06	0.27	0.79
1.20E+13	Al cylinder	82,863	2.7	2.24E+05	3.15E-06	1.35	0.34
1.20E+13	Fe cylinder	982,847	7.86	7.73E+06	2.00E-07	2.96	0.34
					Total	5.35	

Table 9: beam dump energy deposition for positive pion production case

Protons/s	component	Component volume (cc)	Component density (g/cc)	Component mass (g)	Energy Density (GeV/g-p)	kW	% error
1.20E+13	graphite	21,890	1.7	3.72E+04	6.05E-06	0.43	0.52
1.20E+13	Al back	18,241	2.7	4.93E+04	1.77E-06	0.17	1.07
1.20E+13	Al cylinder	82,863	2.7	2.24E+05	1.55E-06	0.66	0.52
1.20E+13	Fe cylinder	982,847	7.86	7.73E+06	1.21E-07	1.79	0.46
					Total	3.05	

Table 10: beam dump energy deposition for negative pion production case

From a comparison of Tables 8, 9, and 10, the distribution of energy deposition changes pretty dramatically between the pbar production case and the positive and negative pion production cases. The aluminum cylinder containing the beam dump core receives about 2.5 kW of beam power for the positive pion production case while the energy deposition in the surrounding steel is about 3 kW. Since the existing beam dump core has significant, irreparable water leaks, the beam dump should probably be replaced before beginning operation of the target station for the Muon g-2 experiment. The MARS results indicate that, relative to the existing beam dump, a much shorter water cooled section would be required.

Comparison of Calculations with Beam Operations Data

Extensive beam operating data for systems considered in the foregoing sections is available to compare with the 120 GeV pbar production calculations. Figure 7 shows data from a 12 hour operating period including incident beam power on target, heat removal from the collection lens, collection lens transformer, collimator, pulsed magnet, and beam dump. Average values taken from a stable period from 1600 to 1700 on February 14, 2011 are given in Table 11. In addition, the calculated values of positive and negative pion production can be compared with the pbar production calculations. The agreement between MARS calculations and actual operating data are reasonably good.

Component	Data from pbar production (kW)	MARS 120 GeV for pbar production (kW)	MARS 8 GeV for positive pion production (kW)	MARS 8 GeV on for negative pion production (kW)
Beam on Target	69.6	70	15	15
Combined lens beam and joule heating	6.2	NA	NA	NA
Lens beam heating	NA	1.54	0.38	.038
Lens joule heating	NA	3.7 (75% DG)	9 (12 Hz, 23% DG)	9 (12 Hz, 23% DG)
Combined xfmr beam and joule heating	1.8	NA	NA	NA
xfmr beam heating	NA	0.61	0.45	.045
xfmr joule heating	NA	0.7 (75% DG)	1.5 (12 Hz, 23% DG)	1.5 (12 Hz, 23% DG)
Collimator	7.4	5.3	0.7	0.9
Pulsed Magnet	4.9	4.8	0.54	1.95
Beam Dump	27.1	29.7	5.3	3.0

Table 11: Comparison of beam heating from operating data MARS calculation. Joule heating in the lens and transformer is taken from test station data. Combined joule/beam heating data collected from ACNET can be compared with the sum of MARS beam heating calculations and test station joule heating data.

Summary

Beam heating in the major target station components for three operating modes has been calculated and compared. The results of MARS calculations for pbar production have been compared with target station operating data which are in good agreement. Conclusions are:

1. The existing target is a mechanically robust design which should provide exceptional service life. However, another design may be necessary to provide enhanced yield.
2. Energy deposition in the collection lens due to beam heating is lower by a factor of about 4. Energy deposition due to beam heating in the transformer is also lower by a factor of about 4; however, energy deposition in the transformer core is comparable to pbar production. Since the core is electrically/thermally isolated from the secondary housing, heat removal from the core is

retarded. Results of test stand operation for the collection lens and transformer should include consideration of transformer core heating by the beam.

3. Since energy deposition is significantly reduced for muon g-2 operation, the collimator design is completely sufficient.
4. Since energy deposition is significantly reduced for muon g-2 operation, the pulsed magnet design is completely sufficient.
5. Beam energy deposition in the beam dump is a factor of 6 to 10 lower for muon g-2 than for pbar production. The beam dump has irreparable water leaks. Since energy deposition is still significant, a new water cooled beam dump will be required. The distribution of beam energy for muon g-2 suggests that a shorter water cooled section is required.

Figure 1: MARS model for pbar target station

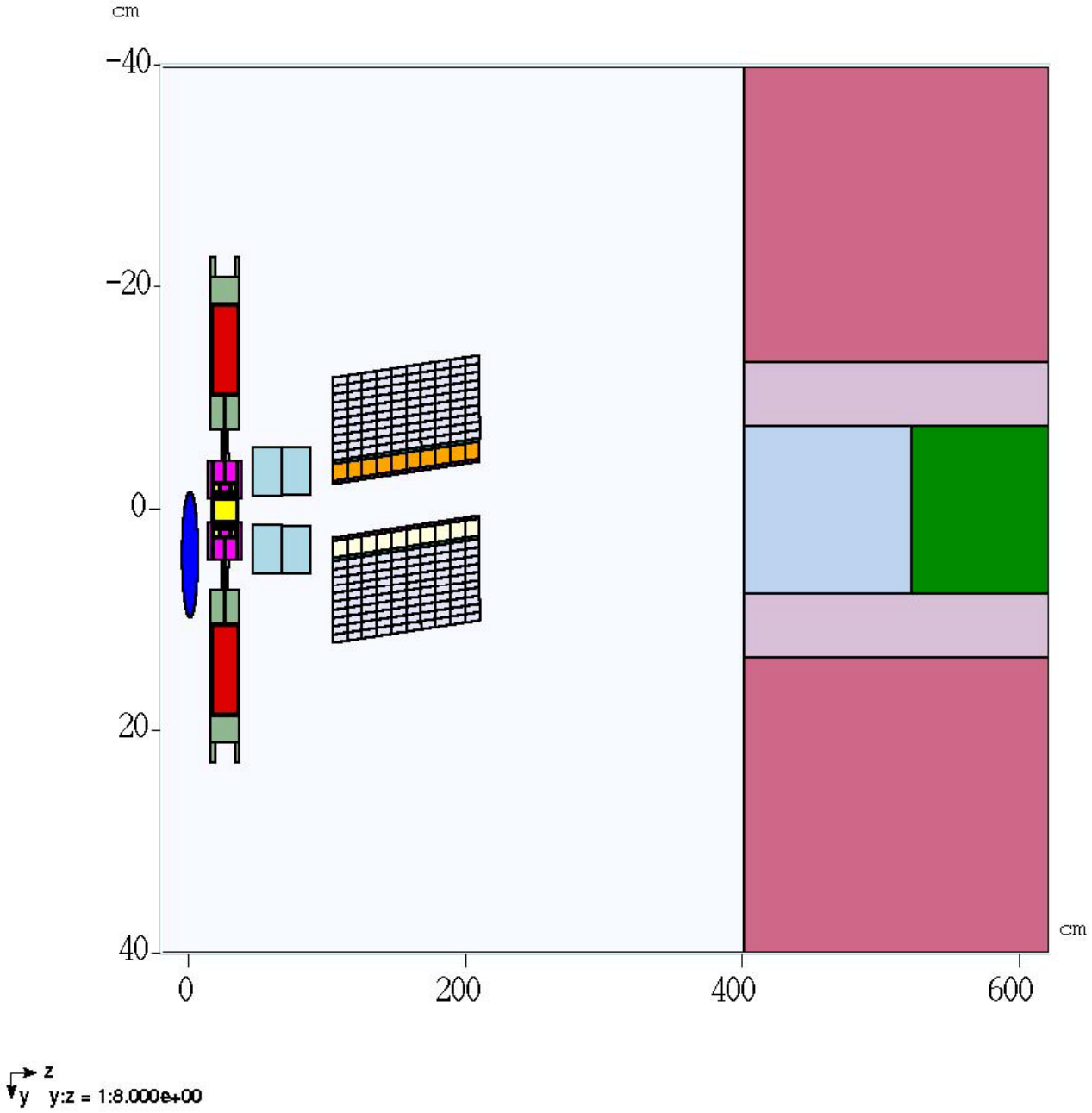

Figure 2: Collection Lens Energy Deposition, Gray/yr for pbar production and g-2 muon pion production

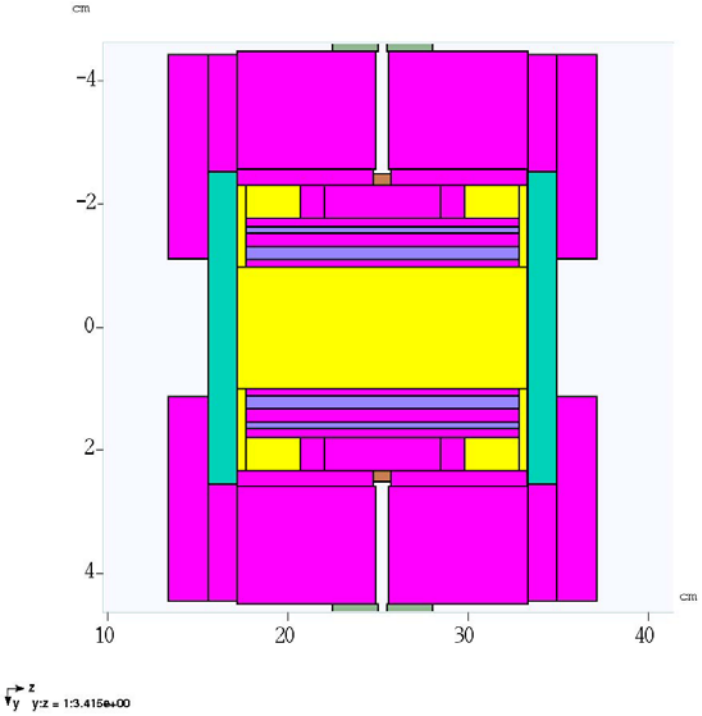

MARS model of collection lens

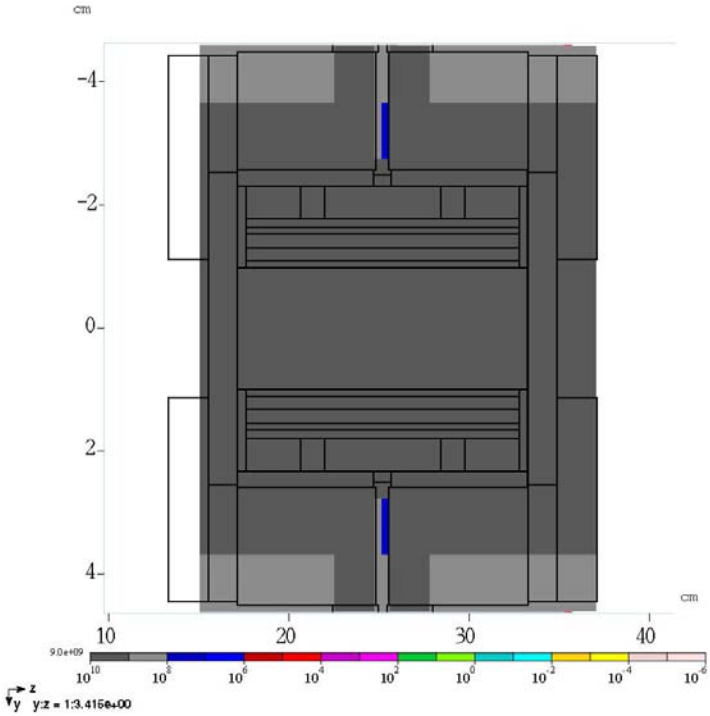

120 GeV, 3.64E 12 p/s pbar production

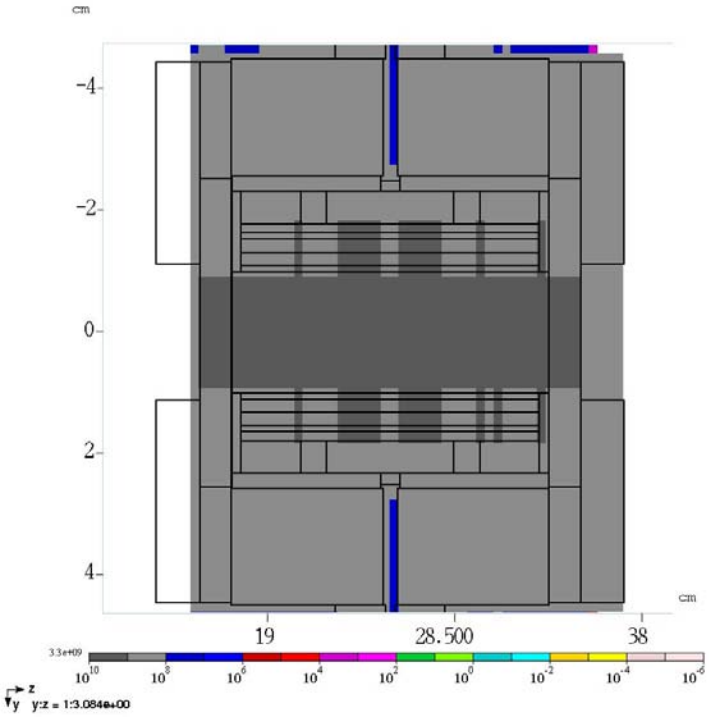

8 GeV, 12E 12 p/s positive pion production

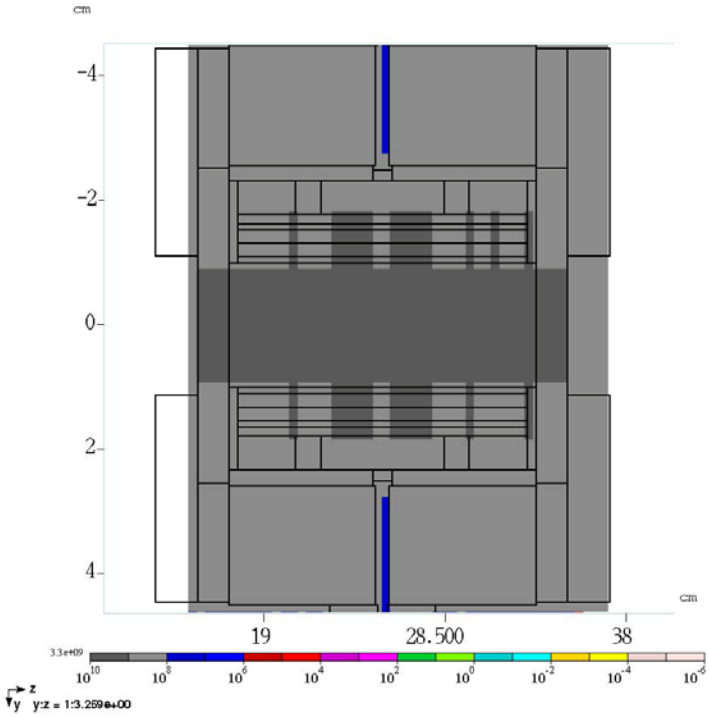

8 GeV, 12E 12 p/s negative pion production

Figure 3: Lens/xfmer Energy Deposition, Gray/yr for pbar production and g-2 muon pion production

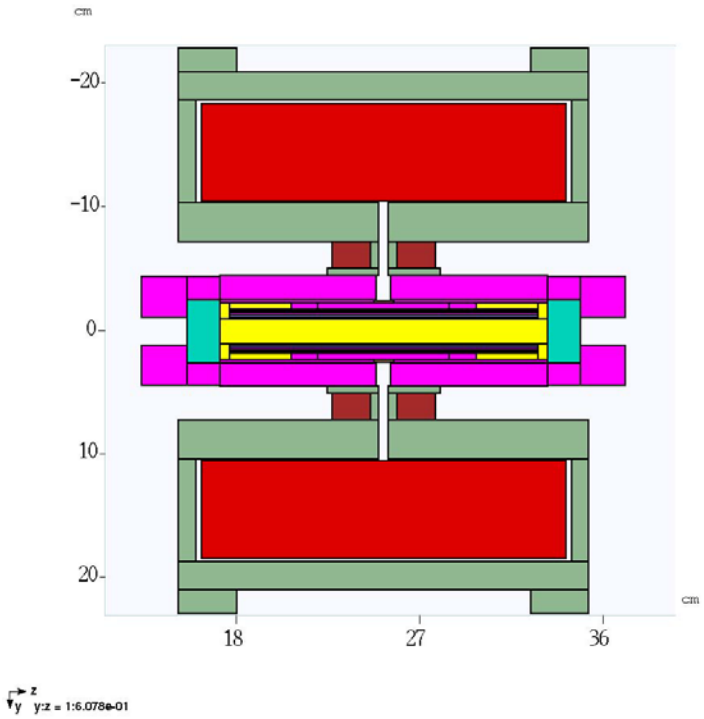

MARS model of lens & transformer

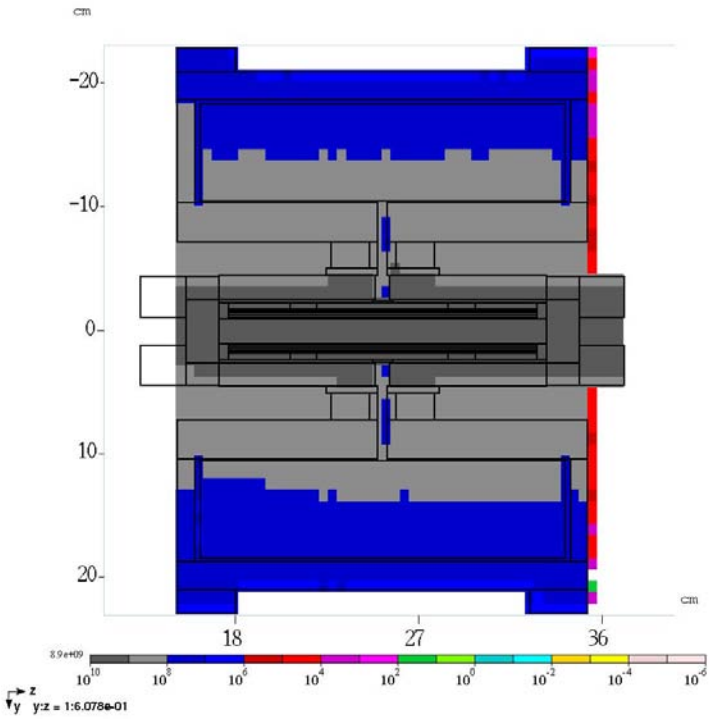

120 GeV, 3.64E 12 p/s pbar production

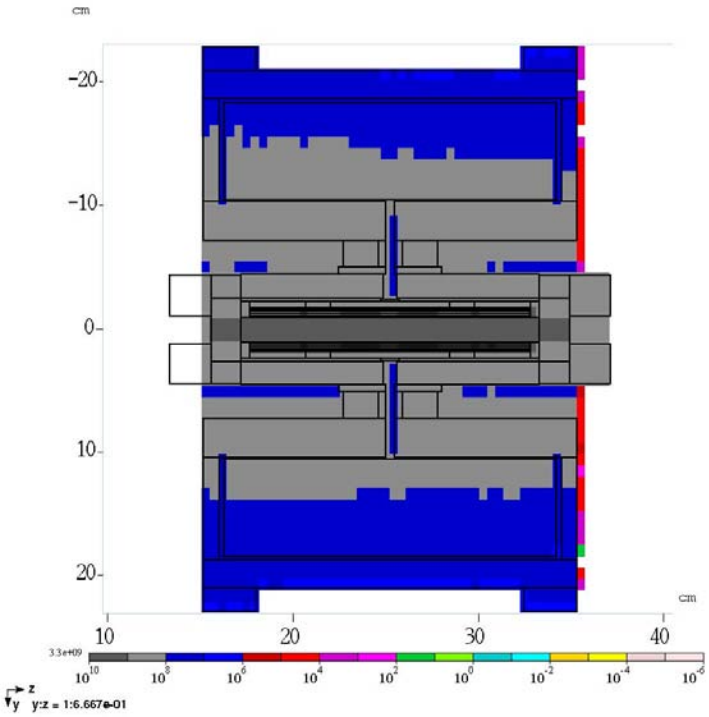

8 GeV, 12E 12 p/s positive pion production

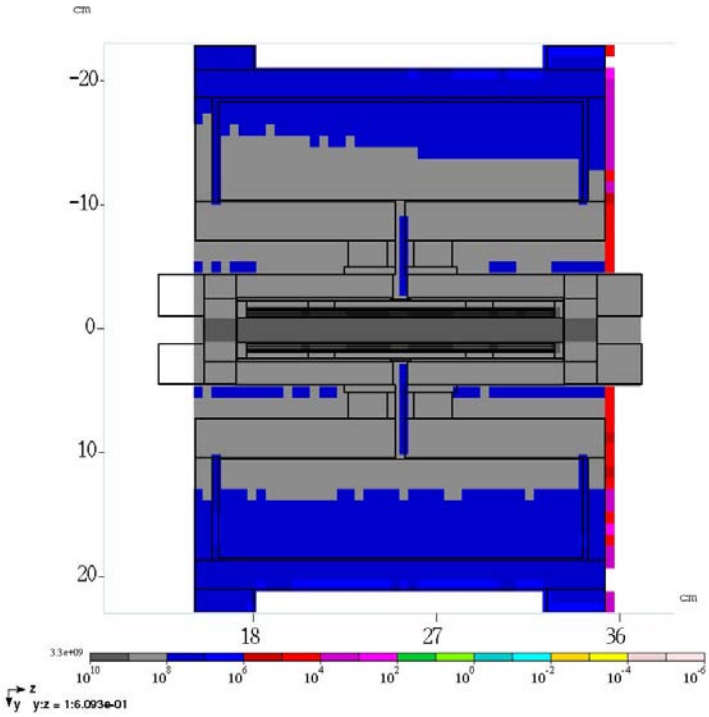

8 GeV, 12E 12 p/s negative pion production

Figure 4: Collimator Energy Deposition, Gray/yr for pbar production and g-2 muon

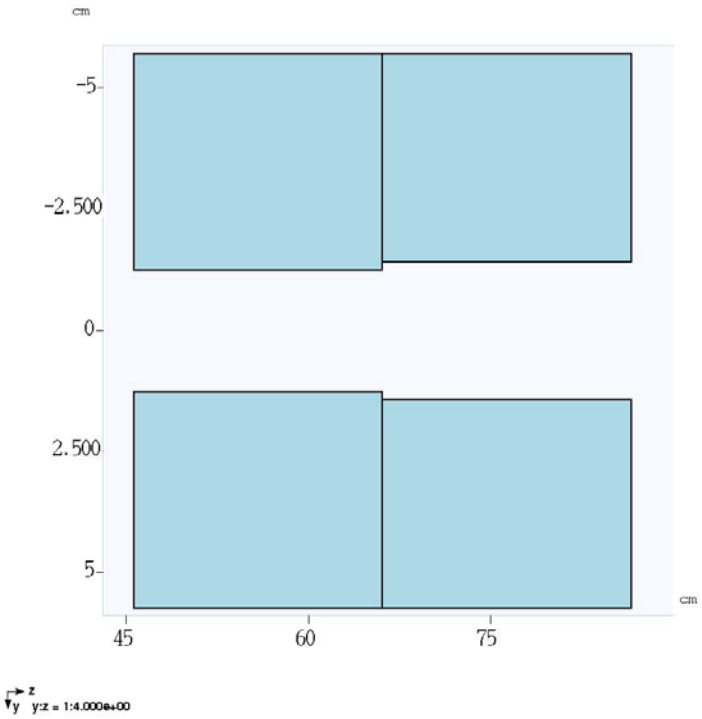

MARS model of collimator

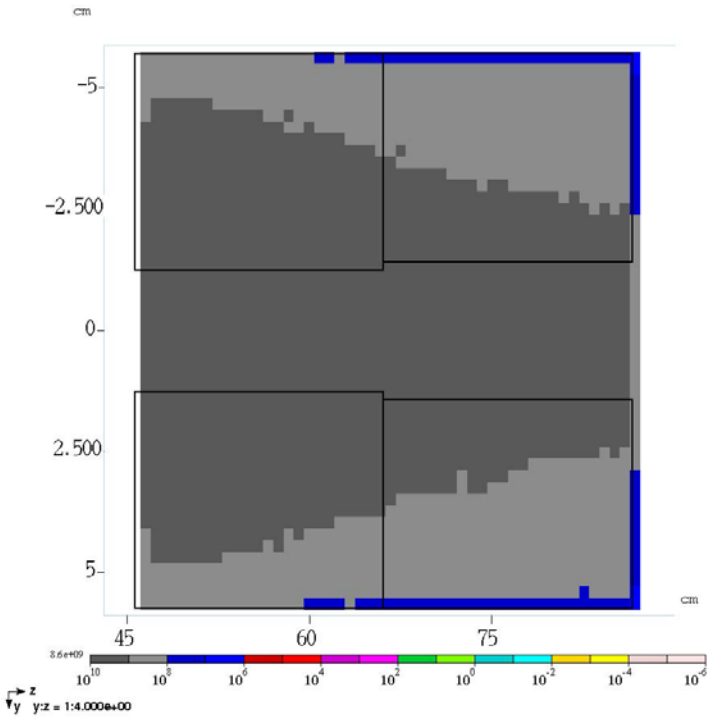

120 GeV, 3.64E 12 p/s pbar production

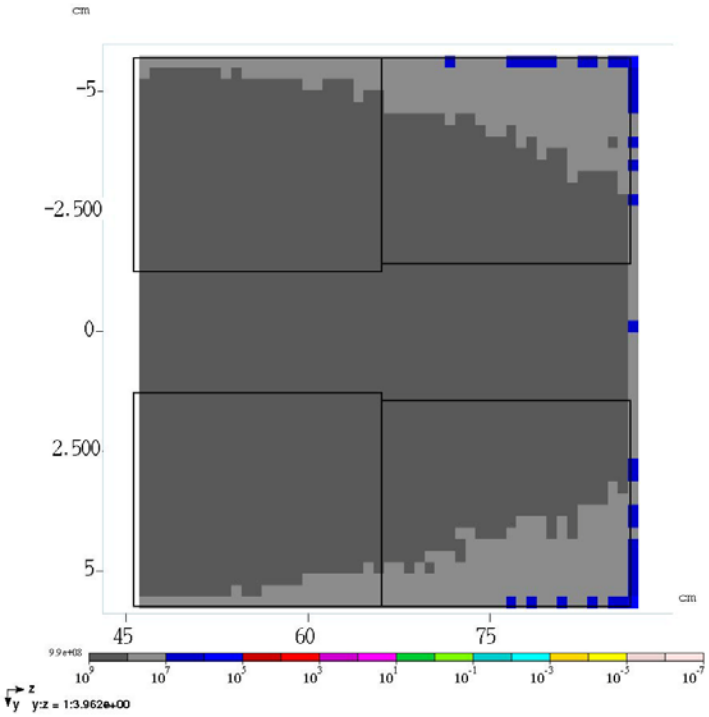

8 GeV, 12E 12 p/s positive pion production

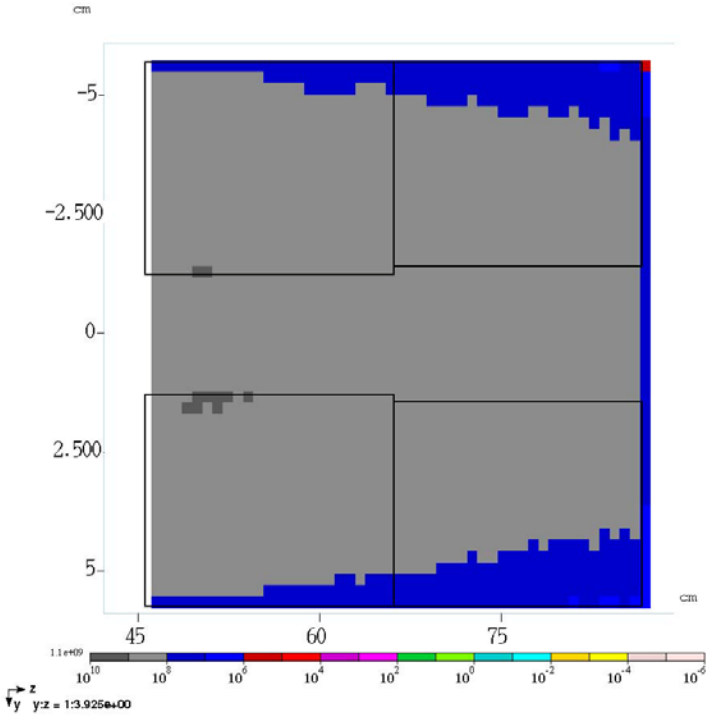

8 GeV, 12E 12 p/s negative pion production

Figure 5: Pulsed Magnet Energy Deposition, Gray/yr for pbar production and g-2 muon

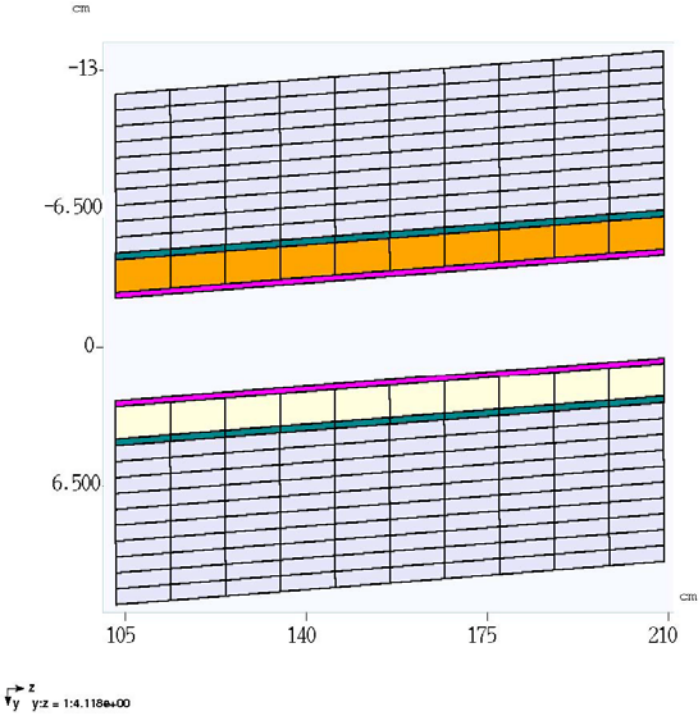

MARS model of pulsed magnet

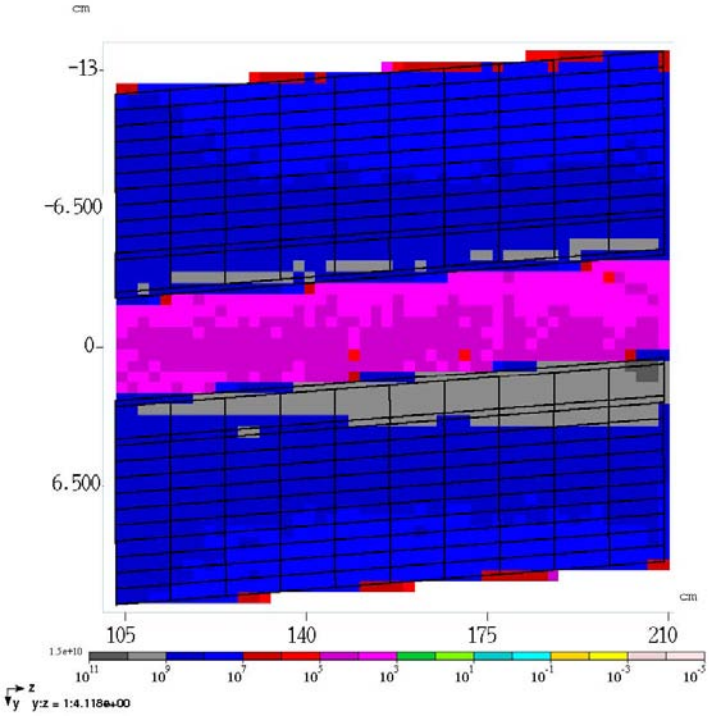

120 GeV, 3.64E 12 p/s pbar production

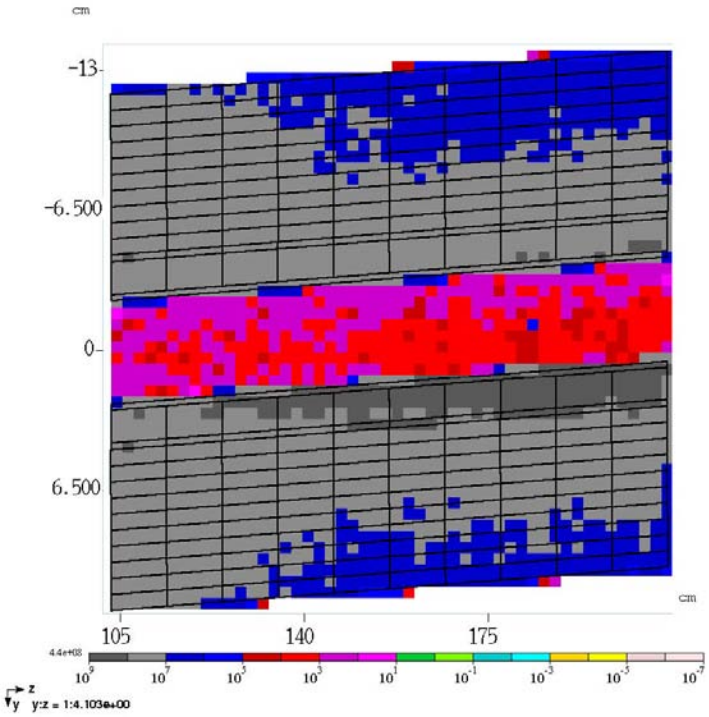

8 GeV, 12E 12 p/s positive pion production

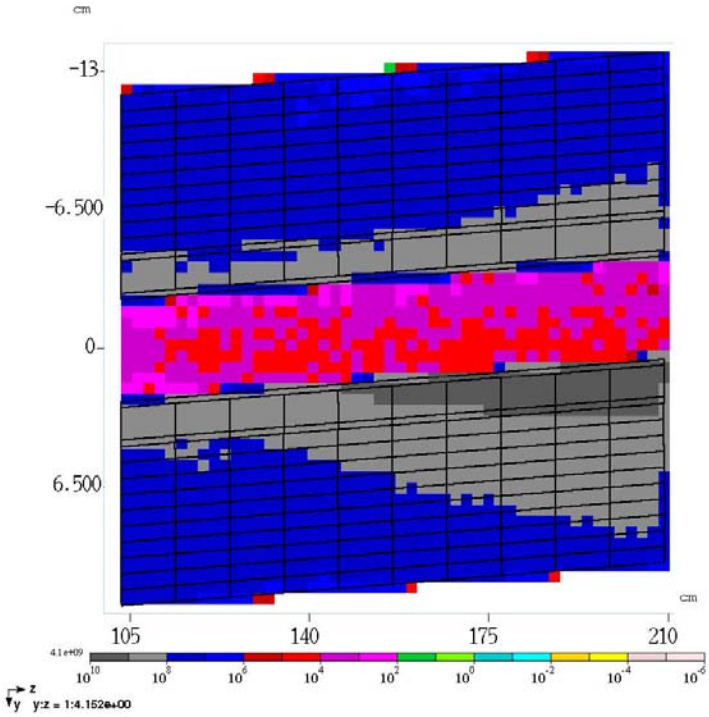

8 GeV, 12E 12 p/s negative pion production

Figure 6: Beam Dump Energy Deposition, Gray/yr for pbar production and g-2 muon

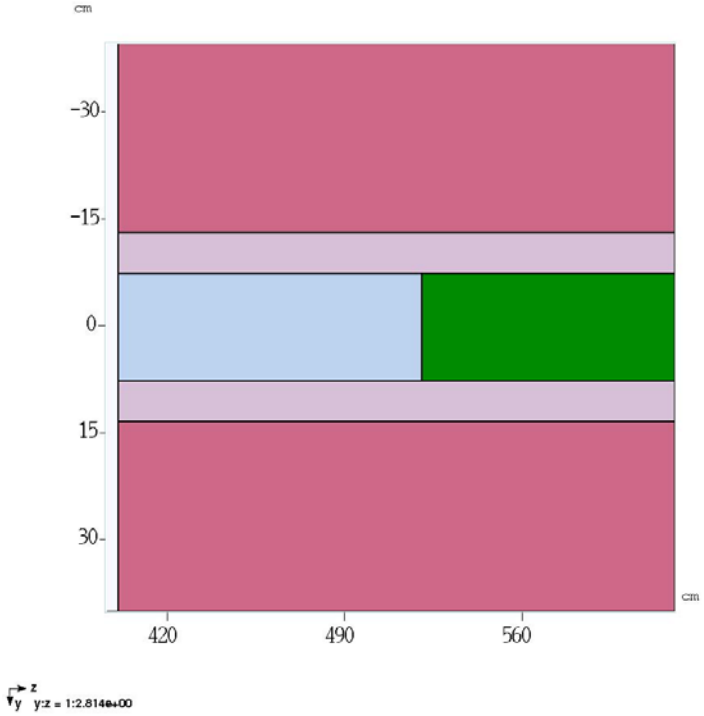

MARS model of beam dump

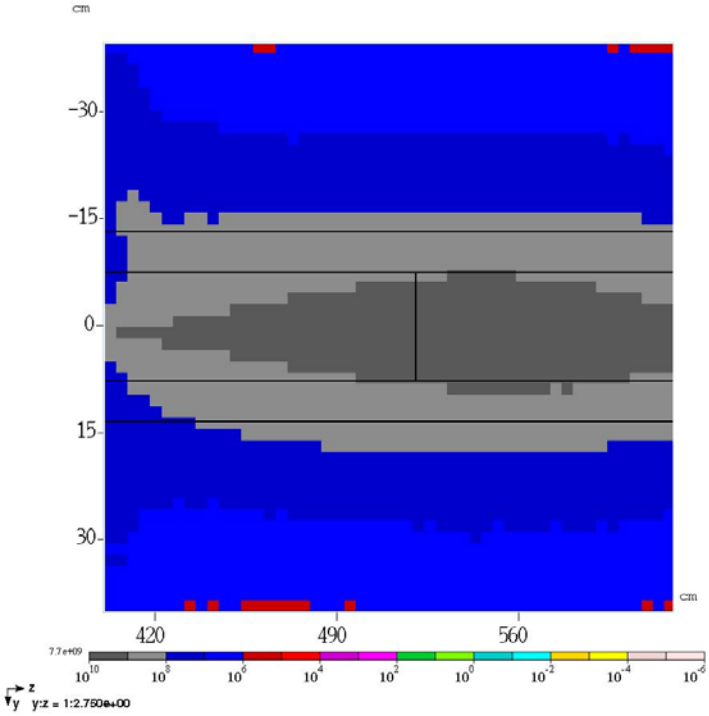

120 GeV, 3.64E 12 p/s pbar production

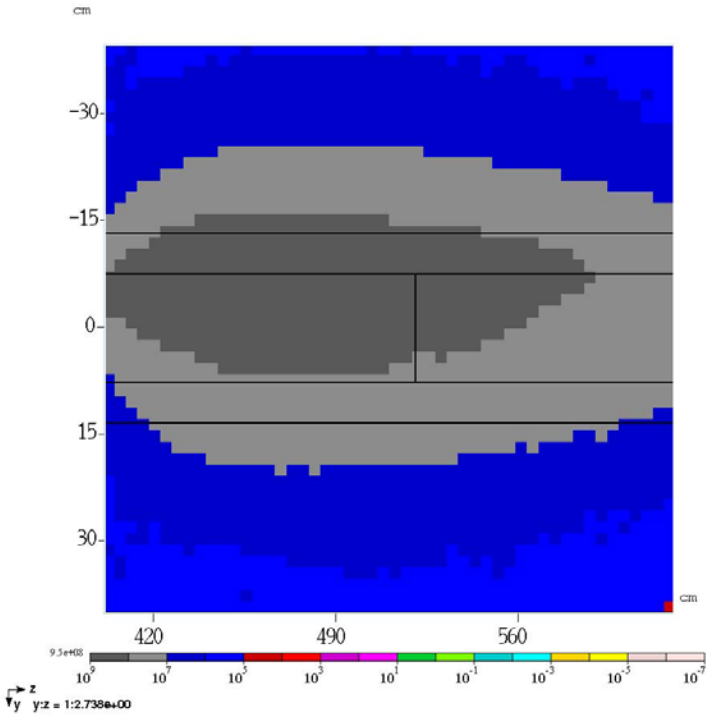

8 GeV, 12E 12 p/s positive pion production

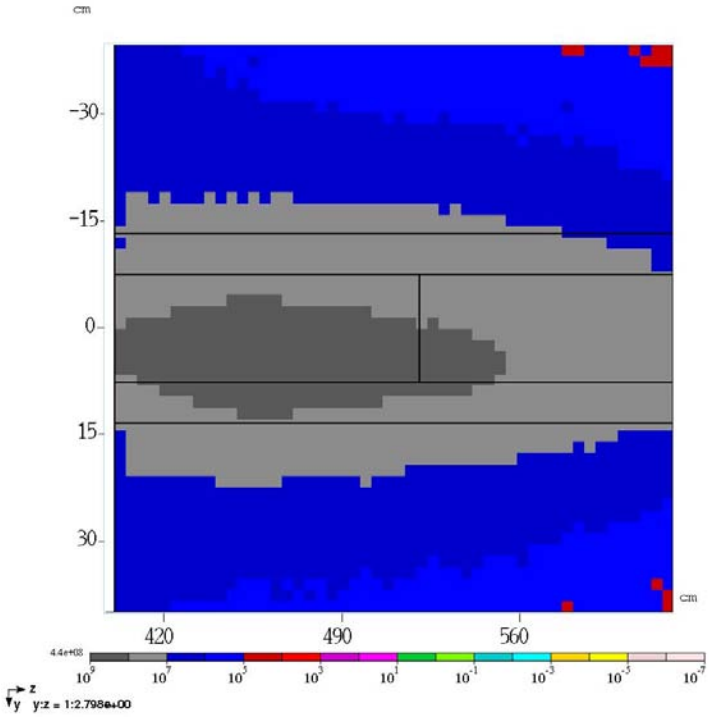

8 GeV, 12E 12 p/s negative pion production

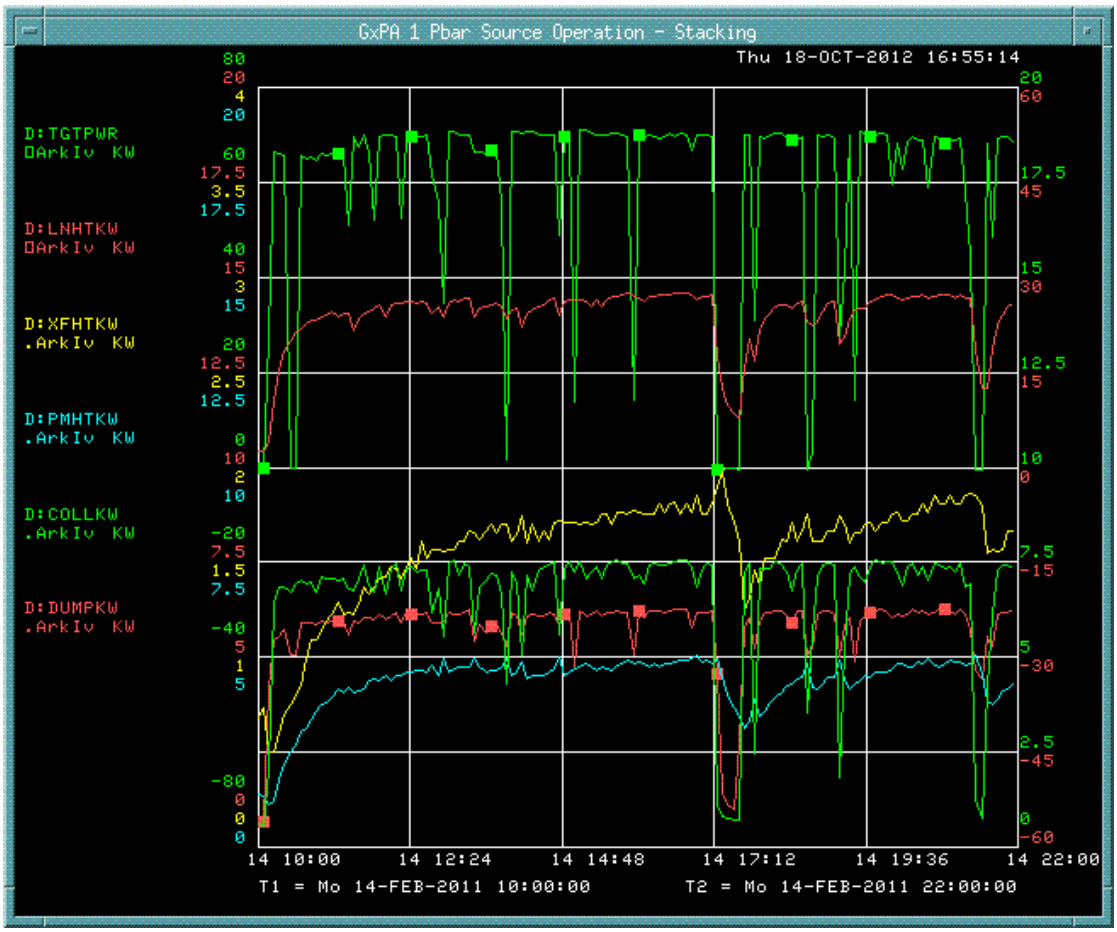

Figure 7: Beam power incident on target and heat removal parameters from various water cooled target station components